Spectroscopic THz near-field microscope

H.-G. von Ribbeck,[1,4,*] M. Brehm,[1] D.W. van der Weide,[2] S. Winnerl,[3] O. Drachenko,[3] M. Helm,[3] and F. Keilmann[1]

[1]*Max-Planck-Institut für Biochemie and Center for Nanoscience, 82152 Martinsried (München), Germany*
[2] *Dept. of Electrical and Computer Engineering, University of Wisconsin, Madison, WI 53706-1691, USA*
[3]*Forschungszentrum Dresden-Rossendorf, 01314 Dresden, Germany*
[4]*Currently with the Institut für Angewandte Photophysik, Technische Universität Dresden, 01062 Dresden, Germany*
[*]*Corresponding author: ribbeck@biochem.mpg.de*

Abstract: We demonstrate a scattering-type scanning near-field optical microscope (s-SNOM) with broadband THz illumination. A cantilevered W tip is used in tapping AFM mode. The direct scattering spectrum is obtained and optimized by asynchronous optical sampling (ASOPS), while near-field scattering is observed by using a space-domain delay stage and harmonic demodulation of the detector signal. True near-field interaction is determined from the approach behavior of the tip to Au samples. Scattering spectra of differently doped Si are presented.

OCIS codes: (180.4243) Near-field microscopy; (300.6495) Spectroscopy, Terahertz; (160.6000) Semiconductor materials.

References and links

1. H. Kuzmany, *Solid-State Spectroscopy* (Springer, Berlin, 1998).
2. T. Kiwa, M. Tonouchi, M. Yamashita, and K. Kawase, "Laser terahertz-emission microscope for inspecting electronic faults in integrated circuits," Opt. Lett. **28**, 2058-2060 (2003).
3. R. Lecaque, S. Gresillon, N. Barbey, R. Peretti, J. C. Rivoal, and A. C. Boccara, "THz near-field optical imaging by a local source," Opt. Commun. **262**, 125-127 (2006).
4. B. Gompf, N. Gebert, H. Heer, and M. Dressel, "Polarization contrast terahertz-near-field imaging of anisotropic conductors," Appl. Phys. Lett. **90**, 82104 (2007).
5. R. Merz, F. Keilmann, R. J. Haug, and K. Ploog, "Nonequilibrium edge-state transport resolved by far-infrared microscopy," Phys. Rev. Lett. **70**, 651-653 (1993).
6. F. Keilmann, "FIR Microscopy," Infrared Phys. and Technol. **36**, 217-224 (1994).
7. S. Hunsche and M. Koch, "THz near-field imaging," Opt. Commun. **150**, 22-26 (1998).
8. U. Schade and K. Holldack, "THz near-field imaging employing synchrotron radiation," Appl. Phys. Lett. **84**, 1422-1424 (2004).
9. B. Knoll and F. Keilmann, "Electromagnetic fields in the cutoff regime of tapered metallic waveguides," Opt. Commun. **162**, 177-181 (1999).
10. F. Keilmann, "Scanning tip for optical radiation," in *U.S. Patent* 4,994,818 (1988),
11. M. Fee, S. Chu, and T. W. Hänsch, "Scanning electromagnetic transmission line microscope with sub-wavelength resolution," Opt. Commun. **69**, 219-224 (1989).
12. F. Keilmann and R. Hillenbrand, "Near-field microscopy by elastic light scattering from a tip," Philos. Trans. R. Soc. London, Ser. A **362**, 787-805 (2004).
13. B. Knoll, F. Keilmann, A. Kramer, and R. Guckenberger, "Contrast of microwave near-field microscopy," Appl. Phys. Lett. **70**, 2667-2669 (1997).
14. S. M. Anlage, D. E. Steinhauer, B. J. Feenstra, C. P. Vlahacos, and F. C. Wellstood, "Near-field microwave microscopy of materials properties," in *Microwave Superconductivity*, H. Weinstock, and M. Nisenoff, eds. (Kluwer, Amsterdam, 2001), pp. 239-269.
15. F. Zenhausern, M. P. O´Boyle, and H. K. Wickramasinghe, "Apertureless near-field optical microscope," Appl. Phys. Lett. **65**, 1623-1625 (1994).
16. F. Keilmann, D. W. v. d. Weide, T. Eickelkamp, R. Merz, and D. Stöckle, "Extreme sub-wavelength resolution with a scanning radio-frequency transmission microscope," Opt. Commun. **129**, 15-18 (1996).
17. B. Knoll and F. Keilmann, "Near-field probing of vibrational absorption for chemical microscopy," Nature **399**, 134-137 (1999).
18. R. Hillenbrand and F. Keilmann, "Complex optical constants on a subwavelength scale," Phys. Rev. Lett. **85**, 3029-3032 (2000).
19. R. Hillenbrand and F. Keilmann, "Material-specific mapping of metal/semiconductor/dielectric nanosystems at 10 nm resolution by back-scattering near-field optical microscopy," Appl. Phys. Lett. **80**, 25-27 (2002).
20. B. Knoll and F. Keilmann, "Infrared conductivity mapping for nanoelectronics," Appl. Phys. Lett. **77**, 3980-3982 (2000).

#91134 - $15.00 USD Received 2 Jan 2008; revised 15 Feb 2008; accepted 17 Feb 2008; published 28 Feb 2008

21. A. J. Huber, D. Kazantsev, F. Keilmann, J. Wittborn, and R. Hillenbrand, "Simultaneous infrared material recognition and conductivity mapping by nanoscale near-field microscopy," Adv. Mater. **19**, 2209-2213 (2007).
22. R. Hillenbrand, T. Taubner, and F. Keilmann, "Phonon-enhanced light-matter interaction at the nanometre scale," Nature **418**, 159-162 (2002).
23. T. Taubner, F. Keilmann, and R. Hillenbrand, "Nanomechanical resonance tuning and phase effects in optical near-field interaction," Nano Lett. **4**, 1669-1672 (2004).
24. S. Schneider, J. Seidel, S. Grafström, L. M. Eng, S. Winnerl, D. Stehr, and H. Helm, "Impact of optical in-plane anisotropy on near-field phonon polariton spectroscopy," Appl. Phys. Lett. **90**, 143101-143101 - 143101-143103 (2007).
25. T. Taubner, R. Hillenbrand, and F. Keilmann, "Nanoscale polymer recognition by spectral signature in scattering infrared near-field microscopy," Appl. Phys. Lett. **85**, 5064-5066 (2004).
26. M. Brehm, T. Taubner, R. Hillenbrand, and F. Keilmann, "Infrared spectroscopic mapping of single nanoparticles and viruses at nanoscale resolution," Nano Lett. **6**, 1307-1310 (2006).
27. N. C. J. v. d. Valk, and P. C. M. Planken, "Electro-optic detection of subwavelength terahertz spot sizes in the near field of a metal tip," Appl. Phys. Lett. **81**, 1558-1560 (2002).
28. P. C. M. Planken, C. E. W. M. Rijmenam, and R. N. Schouten, "Opto-electronic pulsed THz systems," Semiconduct. Sci. Technol. **20**, 121-127 (2005).
29. H. T. Chen, R. Kersting, and G. C. Cho, "THz imaging with nanometer resolution," Appl. Phys. Lett. **83**, 3009-3011 (2003).
30. F. F. Buersgens, H. T. Chen, and R. Kersting, "Terahertz microscopy of charge carriers in semiconductors," Appl. Phys. Lett. **88**, 112115 (2006).
31. P. A. Elzinga, R. J. Kneisler, F. E. Lytle, J. Y., G. B. King, and N. M. Lauredeau, "Pump/probe method for fast analysis of visible spectral signatures utilizing asynchronous optical sampling," Appl. Opt. **26**, 4303-4309 (1987).
32. T. Yasui, E. Saneyoshi, and T. Araki, "Asynchronous optical sampling terahertz time-domain spectroscopy for ultrahigh spectral resolution and rapid data acquisition," Appl. Phys. Lett. **87**, 61101-61101 - 61101-61103 (2005).
33. A. Bartels, A. Thoma, C. Janke, T. Dekorsy, A. Dreyhaupt, S. Winnerl, and M. Helm, "High-resolution THz spectrometer with kHz scan rates," Opt. Express **14**, 430-437 (2006).
34. T. Yasui, Y. Kabetani, E. Saneyoshi, S. Yokoyama, and T. Araki, "Terahertz frequency comb by multifrequency heterodyning photoconductive detection for high-accuracy, high-resolution terahertz spectroscopy," Appl. Phys. Lett. **88**, 241104-241101 - 241104-241103 (2006).
35. A. Bartels, R. Cerna, C. Kistner, A. Thoma, F. Hudert, C. Janke, and T. Dekorsy, "Ultrafast time-domain spectroscopy based on high-speed asynchronuous optical sampling," Rev. Sci. Instrum. **78**, 351071-351078 (2007).
36. A. Dreyhaupt, S. Winnerl, T. Dekorsy, and H. Helm, "High-intensity terahertz radiation from a microstructured large-area photoconductor," Appl. Phys. Lett. **86**, 121114-121111 - 121114-121113 (2005).
37. W. L. Chan, J. Deibel, and D. M. Mittleman, "Imaging with terahertz radiation," Rep. Prog. Phys. **70**, 1325-1379 (2007).
38. L. M. Matarrese and K. M. Evenson, "Improved coupling to infrared whisker diodes by use of antenna theory," Appl. Phys. Lett. **17**, 8-10 (1970).
39. B. Knoll and F. Keilmann, "Enhanced dielectric contrast in scattering-type scanning near-field optical microscopy," Opt. Commun. **182**, 321-328 (2000).
40. M. Brehm, A. Schliesser, and F. Keilmann, "Spectroscopic near-field microscopy using frequency combs in the mid-infrared," Opt. Express **14**, 11222-11233 (2006).
41. A. Cvitkovic, N. Ocelic, and R. Hillenbrand, "Analytical model for quantitative prediction of material contrasts in scattering-type near-field optical microscopy," Opt. Express **15**, 8550-8565 (2007).
42. M. B. Raschke, and C. Lienau, "Apertureless near-field optical microscopy: tip-sample coupling in elastic light scattering," Appl. Phys. Lett. **83**, 5089-5091 (2003).
43. M. Brehm, "Infrarot-Mikrospektroskopie mit einem Nahfeldmikroskop," Dissertation, Fakultät für Physik, Technische Universität, München, p. 128 (2006).
44. N. Ocelic and R. Hillenbrand, "Subwavelength-scale tailoring of surface phonon polaritons by focused ion-beam implantation," Nature Mater. **3**, 606-609 (2004).
45. F. Keilmann and R. Hillenbrand, "Mirror optic for near-field optical measurements," *patent DE 102006002461* filed 18.1.2006 (US filed 16.1.2007, 2006).

1. Introduction

Sub-micrometer-resolved imaging with THz radiation is desirable for specific material contrast that cannot be obtained in other parts of the electromagnetic spectrum. One example of practical interest is the Drude response of lightly doped semiconductors.[1] It exhibits a characteristic edge signature in the THz region from which the carrier density can be derived, and thus THz near-field spectroscopy could well assess the carrier density map with micro- or ultimately nanometer spatial resolution.

#91134 - $15.00 USD Received 2 Jan 2008; revised 15 Feb 2008; accepted 17 Feb 2008; published 28 Feb 2008

Classical free-space focusing of THz waves cannot be expected to yield better than about 100 μm spatial resolution. A sizable improvement has been demonstrated with THz emission,[2, 3] or THz modulation through laser-induced free carriers,[4] both induced by a visible-light focus. Near-field microscopy (SNOM) of *aperture type* has resulted in λ/10 resolution at THz frequencies,[5-7] and has been used with a synchrotron light source.[8] But its further resolution improvement is severely limited by cutoff loss in the tip of a tapered, hollow metal waveguide.[9] An interesting alternative is a non-cutoff waveguide tip, a coaxial guide,[10] as has been shown for millimeter waves,[11] and as demonstrated in an early experiment of reaching λ/20 confinement at 1 THz.[6]

Very high resolution of sub-micrometer scale is certainly achievable by using THz near-field microscopy of *apertureless type* because this concept has not only provided 20-nm resolved SNOM at higher frequencies in the mid-infrared,[12] but also 200 nm resolution with lower-frequency microwaves.[13, 14] The basic idea is the use of a sharp tip as in atomic force microscopy (AFM) and illuminate it with a focused light beam, thereby creating a superfocus with a size of the tip radius to probe the nearby sample's optical properties. Usually scattered light is detected, hence the name s-SNOM for scattering-type SNOM that was first demonstrated in the visible,[15] then with radio waves.[16] A simple theoretical formulation (point-dipole/image-dipole model)[17] has been confirmed to adequately describe the *relative contrast* between different sample materials, by analyzing images taken with visible s-SNOM of metal/dielectric nanostructures,[18, 19] and furthermore with mid-infrared s-SNOM of free carriers,[20, 21] of polar crystals,[22-24] of vibrationally resonant polymers,[25] and of viruses.[26] The first apertureless THz SNOM mapped the near field just below a sharp metal wire tip, inside an optically nonlinear substrate by electro-optic detection.[27] A thin crystal placed between tip and sample modified the measured THz spectrum at the crystal phonon resonance.[28] A THz s-SNOM using forward-scattering[29] was used to detect local electromodulation in a semiconductor surface depletion layer.[30]— Here we describe a broadband THz s-SNOM which detects side-scattering interferometrically, and employs harmonic signal demodulation to suppress background scattering from the tip shaft.

2. Setup

Our setup is based on a tapping-mode AFM complemented with a THz scattering channel. Two THz spectrometer schemes, namely conventional space-domain scanning and time-domain asynchronous optical sampling (ASOPS)[31-35], are installed with a common electro-optic (e.o.) sampling [28] receiver setup (Fig. 1). With this receiver both the amplitude and phase of the THz electric field are recorded as a function of time. Subsequent Fourier transformation determines both the amplitude and phase spectrum of the THz radiation. For near-field measurements we employ harmonic signal demodulation, previously employed in *monochromatic* s-SNOMs,[18] and use a motorized delay stage to vary the delay between the THz pulses and the near-infrared probe pulses used for e.o. sampling. For adjustment and alignment we use ASOPS. Here the probe beam for e.o. sampling is provided by a second femtosecond laser, which is running at a slightly different repetition rate compared to the laser providing the beam for excitation of the THz emitter. This allows a fast sweep of the time delay between THz and probe pulses without any moving components and returns THz spectra at a rate exceeding 20 s^{-1}. Although ASOPS allows a much faster scan of the THz pulse shape signal it has the drawback that lock-in-amplifier-based detection at the tapping frequency and its harmonics is not possible. The femtosecond laser is a Ti:sapphire laser (FemtosourceCompact, FemtoLasers) emitting 10-fs pulses at 800 ± 50 nm wavelength, at 125 MHz repetition rate. Its 500 mW quasi-c.w. beam is weakly focused by an f_1 = 400 mm lens onto a THz emitter[36] (Tera-SED large area emitter, Gigaoptics), biased at 10 V, to produce a 0.2–3 THz output beam. A f_{eff} = 25 mm paraboloidal mirror is used for collimation, and the polarization is vertical. The AFM is home-built with the sample scanned under the vertically vibrating ("tapping") but stationary tip. After 170 mm travel the THz beam is focused to the AFM tip by an f = 10 mm paraboloidal mirror m_1 which is also used for

#91134 - $15.00 USD Received 2 Jan 2008; revised 15 Feb 2008; accepted 17 Feb 2008; published 28 Feb 2008

collimating the side-scattered THz radiation (Fig. 1). This particular geometry allows us to work without the beam splitter that is commonly used in back-scattering s-SNOMs,[12, 18] a notable advantage for broadband-spectroscopic applications where beam splitters with spectrally flat performance are hard to achieve.

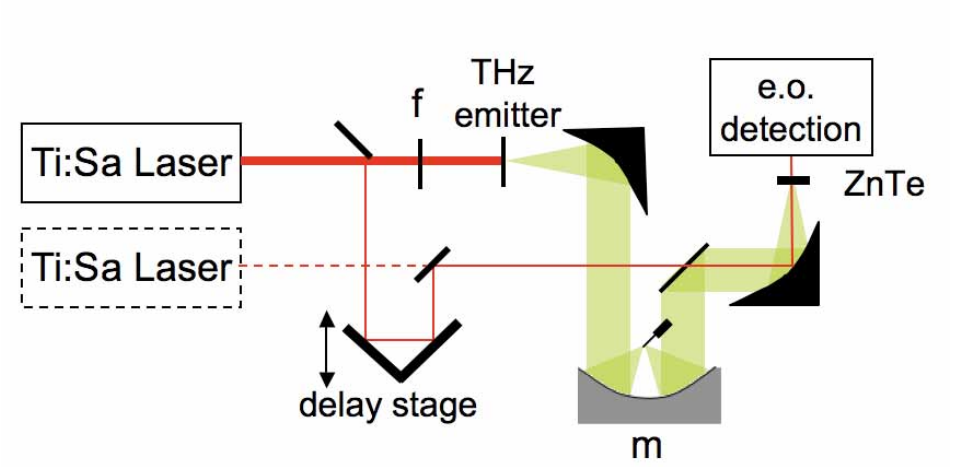

Fig. 1. Optical layout of spectroscopic THz s-SNOM. A common paraboloid mirror m_1 serves for both focusing to the tip and for recollimating THz radiation scattered by about 90° sideways.[45] The THz beam is generated by driving a GaAs emitter with Ti:sapphire laser pulses, and is detected by a standard e.o. setup. A second Ti:sapphire laser (dashed frame) serves to provide a purely time-domain delay, resulting in rapid sequence of spectra. This ASOPS mode is used for s-SNOM alignment. THz s-SNOM operation proceeds by using space-domain delay, involving the delay stage shown but not the second laser.

For scanning tips we use a 65 µm diameter W wire glued to a small Si chip, bent by tweezers and etched electrochemically in 3 mol/l NaOH (3 V_{dc}) to achieve a tip radius in the range 50-300 nm (Fig. 2.) For ASOPS mode we superimpose the attenuated beam of a second, almost identical Ti:sapphire laser using an ITO coated glass plate (TS-GSHR, Bioscience Tools). Both beams are focused with an f_{eff} = 25 mm paraboloidal mirror onto a 1 mm ZnTe crystal for e.o. detection.[28] The THz beam's travel distance from the tip is 190 mm. The repetition rate of the second laser is suitably offset, usually by 375 Hz. At this setting the THz spectrum is down-converted by the factor 125 MHz/ 375 Hz = 333,333 so that 1 THz appears at 3 MHz, and the whole spectrum up to 3 THz fits into the 10 MHz bandwidth of the balanced detector (2107, New Focus). The detector's output is recorded on a scope which is also capable of calculating the Fourier transform (Wavesurfer 422, LeCroy) at a convenient rate of 20 s^{-1}. ASOPS transients and THz spectra are readily observed.

#91134 - $15.00 USD Received 2 Jan 2008; revised 15 Feb 2008; accepted 17 Feb 2008; published 28 Feb 2008

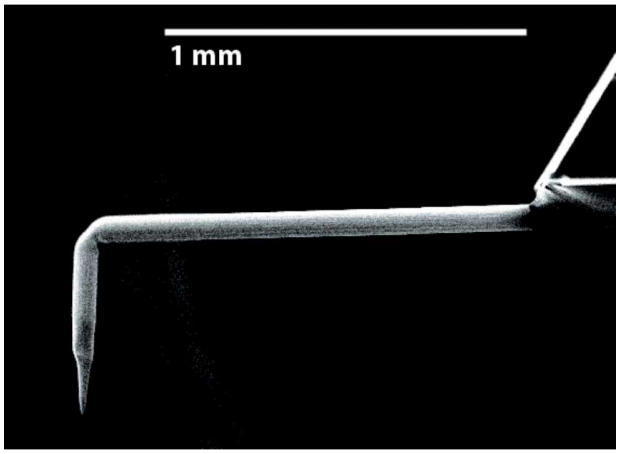

Fig. 2. SEM image of hand-made cantilevered s-SNOM probe for tapping-mode operation, made of 65 μm W wire by bending and electrochemically etching to a tip radius below 500 nm.

3. Experimental results

Figure 3 shows the experimental results. The input spectrum was obtained by placing a mirror pair in the path before the s-SNOM paraboloid, and accordingly translating the delay mirrors. Both the input as well and the direct scattered spectrum (with an Au sample contacting the tip) are found to have essentially the same shape. From this we infer that the tip is a rather broadband antenna. In particular, it does not show an amplitude decrease with rising frequency as reported when using long tips with lengths >> λ.[37] The scattered amplitude is about 3 % of the input amplitude, which means that the power efficiency of side-scattering is only 0.1 %. This is much less than expected from the angular aperture of the paraboloidal mirror which collects as much as 12 % of the scattered radiation when the scattering is isotropic into the half space above a fully reflecting sample. Note that a very weak modulation has also been reported for forward-scattering THz s-SNOM.[30] Therefore, it seems there is much room left for improving the coupling of the THz beam to the tip by systematically engineering its antenna properties, as already accomplished in an earlier, pioneering use of nano-focusing of THz beams by appropriately dimensioned and oriented "catwhisker" antennas.[38]

For detecting the near-field part of the scattered signal we employ a differential method, anticipating that most of the scattering probably would stem from "background" scattering centers on the shaft not radiatively connected with the tip apex. As shown earlier, demodulating the detector signal at a low harmonic of the tapping frequency is an excellent means of effectively suppressing this unwanted background scattering.[18, 39] This principle can well be adapted for broadband frequency-comb operation as we showed recently in the mid-infrared, by first taking spectra in rapid sequence, then calculating differences according to their momentary tip-sample distances.[40] This approach holds great promise for future experiments when advanced digitizing and computing methods become available. Here though we demonstrate, alternatively, that the spectrally-integrated scattering signal can first be demodulated and then be recorded as a function of mechanical delay; a second laser is not needed. For this method we split off a weak (5 % power) reference beam from the first laser beam, by a metallized mirror with a sharp edge, which we delay with a cube corner mirror on a motorized translation stage (Fig. 1). A total mirror scan over 1100 μm is used at a velocity of 1 μm/s, resulting in a total recording time of 19 min. The 1100 μm spatial displacement of the mirror translates into a time delay of the THz pulse over 7.35 ps which results in a frequency resolution of 0.14 THz in the spectrum after Fourier transformation of the transient signal. With the mirror positioned for zero delay, we find that the demodulated signal is rather

#91134 - $15.00 USD Received 2 Jan 2008; revised 15 Feb 2008; accepted 17 Feb 2008; published 28 Feb 2008

robust against misadjustment of the paraboloidal mirror, and increases linearly with the tapping amplitude.

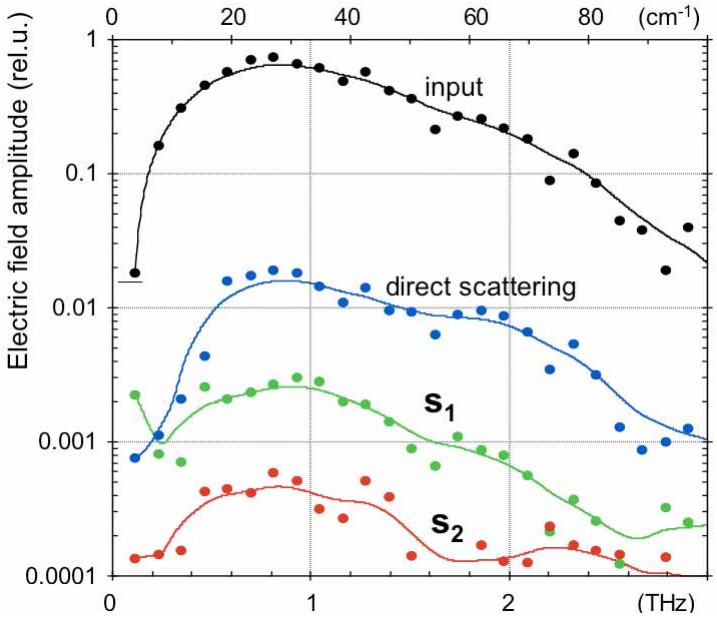

Fig. 3. Experimental THz s-SNOM spectra of Au using the space-domain delay method (no averaging). The input spectrum is obtained by placing a mirror pair before the focusing paraboloid. This and the direct scattering spectra are taken at 5x speed. The first (s_1) and second-order demodulated scattering spectra (s_2) are shown. In all spectra (including those in Figs. 4,5) the data points are from measurement, the curves are obtained by weighted smoothing.

A necessary and sufficient experimental proof of near-field interaction is the occurrence of a steeply rising scattering amplitude when a sample is approached. This is predicted by the point-dipole model and routinely monitored in visible and mid-infrared s-SNOMs, whereby the length scale of this increase directly tells the lateral spatial resolution.[19, 39] With a maximized demodulated THz signal near zero delay we slowly deproach the sample and record the signal changes. Figure 4 shows that the amplitude rises from its 90 % ("set point") value to that of its free oscillation, 300 nm_{pp}, while the THz signal decreases when demodulated at both the tapping frequency ≈ 15 kHz (s_1) or at its second harmonic (s_2). In this experiment the lock-in time constant was 300 ms, and the deproach speed was 4.5 nm/s. Since the s_1 signal does not fall to zero at large distance we conclude it is contaminated by background scattering. The s_2 signal, however, is clearly dominated by near-field interaction. The s_2 decay occurs somewhat more steeply than the near-field part of the s_1 signal, in accordance with former experience in the mid-infrared.[39] The tip size inferred from Fig. 4 is of the order of 200-300 nm, agreeing with SEM observation.

#91134 - $15.00 USD Received 2 Jan 2008; revised 15 Feb 2008; accepted 17 Feb 2008; published 28 Feb 2008

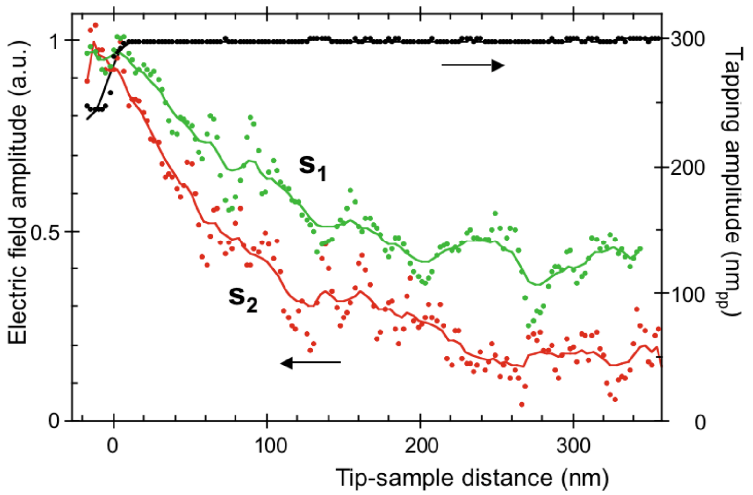

Fig. 4. Approach curves of demodulated THz signals using a W tip (radius 300 nm) on a flat Au sample (three curves averaged). The tapping amplitude reduces when contact is made. The THz field amplitude decays at a characteristic distance from the sample, giving the range of near-field interaction which is connected to the attainable spatial resolution.

With the tapping tip in contact we record delay curves of the demodulated THz signal, and compute by Fourier transformation the s_1 and s_2 spectra presented in Fig. 3. Interestingly the s_1 spectrum is similar in shape to the input and the direct scattering spectra. The s_2 spectrum has barely sufficient signal-to-noise ratio for such a comparison. Clearly an improvement of the signal is needed, possibly by a higher THz power or by a better antenna shape and alignment. Note that THz spectroscopy has the exceptional potential to span a very large frequency range of about four octaves (0.2-3.2 THz), much wider than has been accessible with a mid-infrared comb spectrum that has spanned only a third of an octave (28-35 THz).[40]

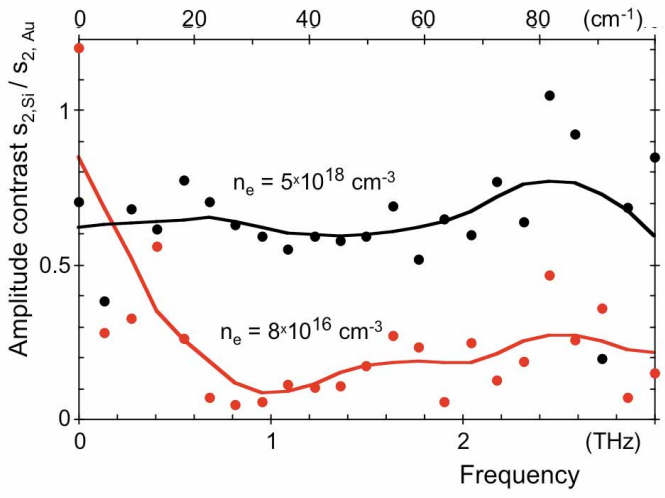

Fig. 5. Experimental THz s-SNOM amplitude-contrast spectra (s_2) of doped Si, normalized to Au (experimental dots; the dashed curves are guides to the eye).

#91134 - $15.00 USD Received 2 Jan 2008; revised 15 Feb 2008; accepted 17 Feb 2008; published 28 Feb 2008

In view of the presently attained signal-to-noise ratio a true sample scanning is not yet practical. We report instead measured THz s-SNOM spectra of different materials. For this we evaporated patches of 100 nm thick Au film on doped Si samples and took s_2 spectra on both materials to compute spectra of relative contrast. The results in Fig. 5 show that highly doped Si has a rather flat amplitude spectrum when referenced to Au, at a level of about 0.6. The lightly doped Si sample has a significantly smaller relative amplitude of about 0.2 for frequencies above 1 THz, but somewhat less at 0.8 THz, and somewhat greater below 0.5 THz. This is explained by the Drude response of free carriers in Si. For comparison we calculate the predicted near-field scattering using the point-dipole model result,[41] modified from earlier formulations[17, 18] by substituting $(1+\beta)$ with $(1+r)^2$ which specifically improves agreement in the case of resonant sample material,[42-44]

$$se^{i\varphi} \propto (1+r)^2 \alpha / (1-\alpha\beta/(16\pi(a+z)^3)), \tag{1}$$

where α is the point-dipole polarizability representing the tip, β is the surface response function representing the sample, a is the tip radius, z is the tip-sample distance, and r is the amplitude reflectivity of the sample. The predicted near-field amplitude contrast spectra of Si vs. Au are shown in Fig. 6, with free electron density as parameter. As observed in Fig. 5 higher concentrations lead to a high scattering with nearly flat spectrum, while indeed lower concentrations lead to a characteristic plasma edge in the THz region. Caution should however be taken in interpreting the data in Fig. 5 as pure near-field spectra, because also background scattering can be contained which is also expected to exhibit a plasma-edge spectrum through the Fresnel reflection factor r that accounts for sample reflection of parts of the illuminating as well as of the background-scattered light. To resolve the uncertainty approach curves should be taken on the Si samples; this is not yet possible due to weaker scattering.

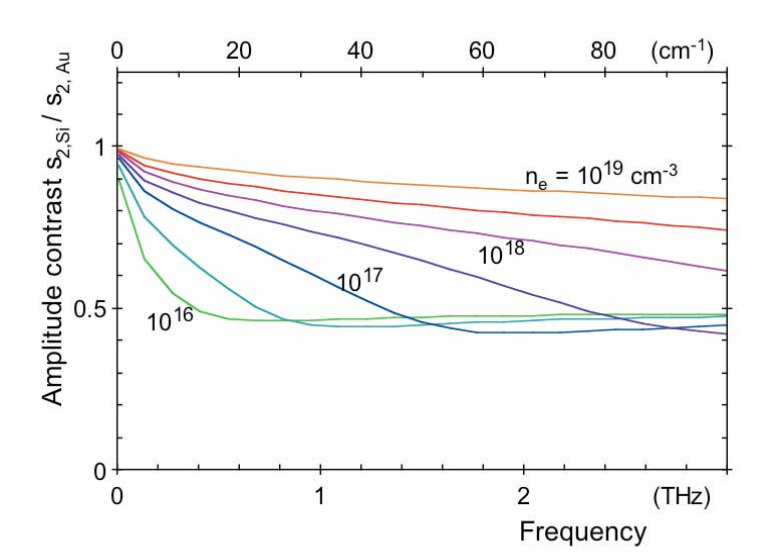

Fig. 6. Theoretical THz s-SNOM amplitude-contrast spectra of doped Si normalized to Au, calculated by the point-dipole/mirror-dipole model for different free electron densities n_e.

4. Conclusion

This experiment shows that broadband THz s-SNOM is achievable with the same measurement technique as previously demonstrated in the mid-infrared, by employing

#91134 - $15.00 USD Received 2 Jan 2008; revised 15 Feb 2008; accepted 17 Feb 2008; published 28 Feb 2008

scattering in a non-forward direction and demodulating the THz signal at the second tapping harmonic to suppress background. Space-domain delay is used to obtain spectroscopic s-SNOM information. Engineering the tip's antenna function should enable higher signals, and thus enable spectroscopic images by THz s-SNOM, to be of benefit to fundamental research into nanoscale composites, nano-structured conductivity phenomena, and metamaterials, and furthermore to enable applications in the chemical and electronics industries.

Acknowledgements

We thank R. Guckenberger, T. Ganz, R. Hillenbrand, A. Huber, and N. Ocelic for help and numerous discussions. Supported by Sonderforschungsbereich 563 "Organische Funktionssysteme auf Festkörpern" of Deutsche Forschungsgemeinschaft, and by AFOSR MURI F49620-03-1-0420, "Nanoprobe Tools for Molecular Spectroscopy and Control".

#91134 - $15.00 USD Received 2 Jan 2008; revised 15 Feb 2008; accepted 17 Feb 2008; published 28 Feb 2008